

# The refined structure of the quinoprotein methanol dehydrogenase from *Methylobacterium extorquens* at 1.94 Å

Minakshi Ghosh<sup>1\*</sup>, Chris Anthony<sup>2</sup>, Karl Harlos<sup>1,3</sup>, Matthew G Goodwin<sup>2</sup>  
and Colin Blake<sup>1,3\*</sup>

<sup>1</sup>Laboratory of Molecular Biophysics, The Rex Richards Building, University of Oxford, South Parks Road, Oxford OX1 3QU, UK, <sup>2</sup>SERC Centre for Molecular Recognition, Biochemistry Department, University of Southampton, Southampton SO16 7PX, UK and <sup>3</sup>Oxford Centre for Molecular Sciences, University of Oxford, Oxford OX1 3QU, UK

**Background:** Methanol dehydrogenase (MDH) is a bacterial periplasmic quinoprotein; it has pyrrolo-quinoline quinone (PQQ) as its prosthetic group, requires Ca<sup>2+</sup> for activity and uses cytochrome *c*<sub>L</sub> as its electron acceptor. Low-resolution structures of MDH have already been determined.

**Results:** The structure of the  $\alpha_2\beta_2$  tetramer of MDH from *Methylobacterium extorquens* has now been determined at 1.94 Å with an R-factor of 19.85%.

**Conclusions:** The  $\alpha$ -subunit of MDH has an eight-fold

radial symmetry, with its eight  $\beta$ -sheets stabilized by a novel tryptophan docking motif. The PQQ in the active site is held in place by a coplanar tryptophan and by a novel disulphide ring formed between adjacent cysteines which are bonded by an unusual non-planar *trans* peptide bond. One of the carbonyl oxygens of PQQ is bonded to the Ca<sup>2+</sup>, probably facilitating attack on the substrate, and the other carbonyl oxygen is out of the plane of the ring, confirming the presence of the predicted free-radical semiquinone form of the prosthetic group.

**Structure** 15 February 1995, **3**:177–187

Key words: calcium, disulphide bridge, methanol dehydrogenase, PQQ, quinoprotein

## Introduction

Methanol dehydrogenase (MDH) is a soluble quinoprotein which oxidizes methanol to formaldehyde in the periplasm of methylotrophic bacteria growing on methane or methanol [1]. Its prosthetic group is pyrrolo-quinoline quinone (PQQ) [2,3], from which electrons are passed to a specific soluble cytochrome (cytochrome *c*<sub>L</sub>) [4,5]. Relatively little is known about the mechanism by which PQQ is reduced to the quinol (PQQH<sub>2</sub>), but it is probable that the reaction is initiated when the substrate is attacked by an active site base. It has been proposed that the initial attack is followed by hydride transfer to the C5 carbonyl of the PQQ, or by formation of a hemiketal intermediate at the same carbon atom [2,6–8]. Reoxidation of the quinol form of the prosthetic group is achieved by two single electron transfers to the cytochrome *c*<sub>L</sub>. During this process, an intermediate form of the prosthetic group is produced. This is the free-radical semiquinone form, as implied by the electron paramagnetic resonance spectrum of the enzyme as it is normally isolated [9–11]. Nothing is known at present about the route for electron transfer from the quinol to the cytochrome, although there is some evidence that a novel disulphide ring seen in the active site of our lower resolution structure of the enzyme might be involved; when the ring was broken by reduction, all interaction with the cytochrome *c*<sub>L</sub> was lost [12]. This novel disulphide ring structure was formed from adjacent cysteines which appeared (at low

resolution) to be joined by a *cis* peptide, as predicted by Ramachandran and colleagues [13,14].

The low-resolution structure of MDH [12,15] confirmed its  $\alpha_2\beta_2$  tetrameric structure, and indicated that the folding of the  $\alpha$ -chain was similar to that observed in the heavy chain of methylamine dehydrogenase, with a number of 'W'-shaped  $\beta$ -sheets arranged radially like a propeller fold [16]. In the case of methylamine dehydrogenase, there were seven 'blades' or  $\beta$ -sheets, corresponding to what Murzin [17] calculated to be the optimum number for such a folding arrangement; he concluded that "the  $\beta$ -propeller-fold accommodates seven motifs and any additional  $\beta$ -structure would not be included in the propeller domain" [17]. The demonstration that MDH has eight  $\beta$ -sheet motifs in such a propeller fold clearly suggests that there must be some special structural features relating to this in MDH.

This paper presents the 1.94 Å structure of MDH, and provides an explanation of the stable eight-fold propeller fold structure, together with a demonstration that the novel disulphide ring structure in the active site does not contain the predicted *cis* peptide bond, but an unusual non-planar *trans* peptide bond. Also, the structure confirms the predicted role of Ca<sup>2+</sup> in holding PQQ in the required configuration at the active site [11], and indicates the structure of the predicted free-radical form of the prosthetic group. These structural features have obvious

\*Corresponding authors.

implications with respect to the mechanism of the enzyme and provide the background for future understanding of the path of electron transfer in this protein.

## Results and discussion

MDH from the pink facultative methylotroph *Methylobacterium extorquens* was crystallized in two distinct forms as described previously [18]. The three-dimensional structure was solved at 1.94 Å for the triclinic crystals by molecular replacement using the 3 Å model obtained from the orthorhombic crystals. The electron-density map was interpreted with the known sequences of the two subunits [19,20] followed by crystallographic refinement. The R-factor was 19.85% for all data (86 729 reflections) with a free R-factor of 22.93% (4621 reflections). The model showed good stereochemistry; bond lengths and angles have a root mean square (rms) deviation from the standard values of 0.008 Å and 1.59°, respectively.

## Overall structure

The final electron-density maps at 1.94 Å resolution show the complete polypeptide chain of the  $\alpha$ - and  $\beta$ -subunits without breaks but lacking the C-terminal four

residues of the  $\alpha$ -chain and the last residue of the  $\beta$ -chain (Fig. 1). The amino acid sequences of the two chains [19,20] are confirmed by the electron-density maps. These also confirm the presence of one PQQ in the semiquinone form and one  $\text{Ca}^{2+}$  ion in each  $\alpha\beta$  unit. The overall structure of the  $\alpha_2\beta_2$  tetramer is shown in Fig. 2. The tetramer has the shape of a very shallow 'V' with dimensions of 55 Å×55 Å×110 Å. The large  $\alpha$ -subunits are of a nearly spherical pear shape with a diameter of ~55 Å, while the much smaller  $\beta$ -chains have an extended structure lying across the surface of the  $\alpha$ -subunits. The two  $\alpha$ -subunits interact across a large planar interface. Each  $\beta$ -chain interacts with its  $\alpha$ -subunit over its entire length, but makes no contact with the symmetry-related  $\alpha\beta$  unit.

## Structure of the $\alpha$ -subunit

The overall fold of the  $\alpha$ -subunit is a superbarrel (using the nomenclature of Branden and Tooze [21]) composed of eight antiparallel four-stranded  $\beta$ -sheet motifs; these W motifs are stacked radially around a pseudo eight-fold symmetry axis running through the centre of the subunit (Figs 1 and 3). This structure has also been referred to as a propeller fold, each W motif representing a 'propeller blade' [17]. Homologous structures with six, seven and

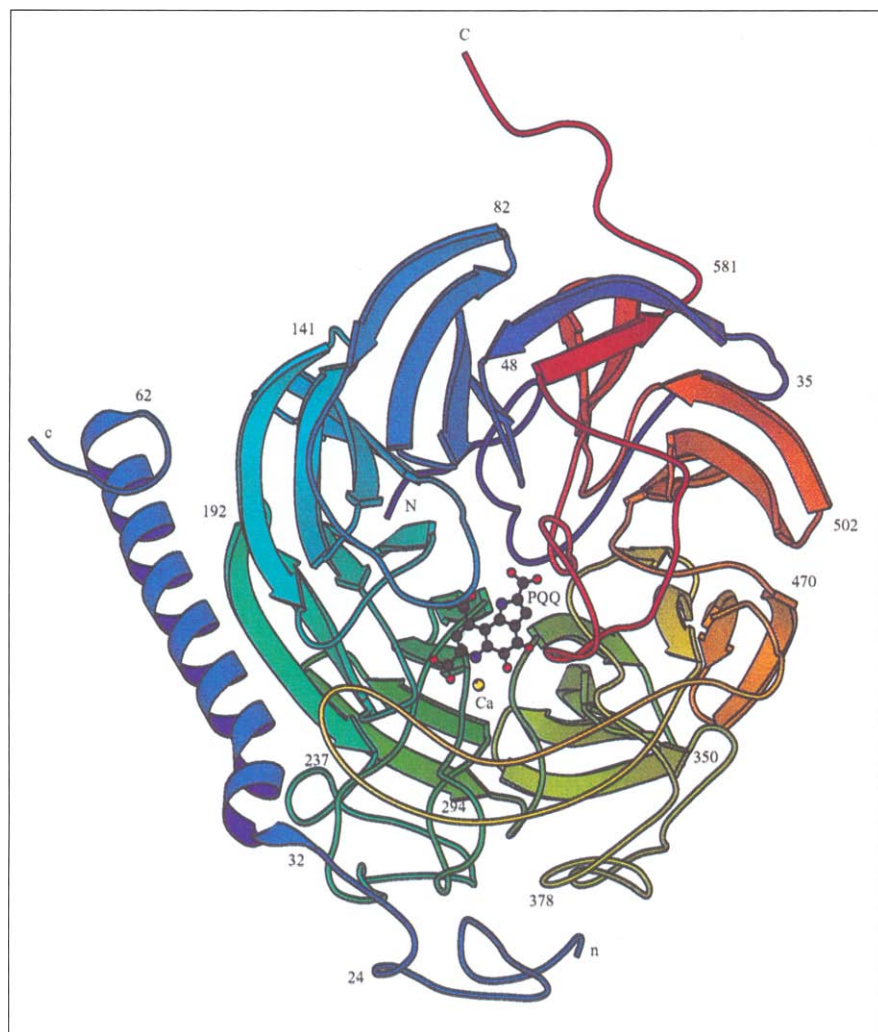


**Fig. 1.** The  $\alpha\beta$  unit of MDH looking down the pseudo eight-fold axis, simplified to show only the  $\beta$ -strands of the eight 'W' motifs of the  $\alpha$ -chain, and the long  $\alpha$ -helix of the  $\beta$ -chain, but excluding other limited  $\beta$ -structures and short  $\alpha$ -helices. The termini of the  $\alpha$ -chain are marked N and C and the those of the  $\beta$  chain n and c. In the  $\alpha$ -chain the colour changes from blue to red as one goes from the N to the C terminus while the  $\beta$ -chain is shown in uniform blue. The outer strand of each W motif is the D strand, the inner strand being the A strand. The W motifs are arranged in this view in an anticlockwise manner. Residue 82 marks the start of the D strand of W1; residue 141 marks the start of the D strand of W2 (and so on), residue 502 marking the start of the D strand of W7. The exceptional motif, W8, is made up of strands A-C near the C terminus plus its D strand (ending at residue 48) from near the N terminus. The PQQ prosthetic group is in skeletal form with oxygen atoms in red. The calcium ion is shown in yellow.

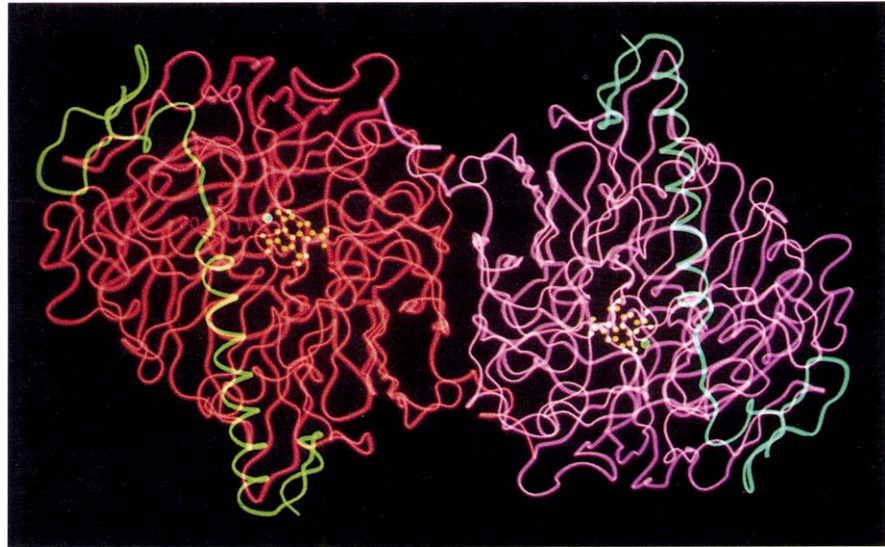


**Fig. 2.** A ribbon drawing of the full  $\alpha_2\beta_2$  tetrameric MDH looking down the molecular symmetry axis. The  $\alpha$ -chains are shown in red and lilac and the  $\beta$ -chains in green and turquoise. The PQQ is shown as yellow circles and the calcium ions as blue circles.

eight of these blades have been described. The neuraminidase from influenza virus has six blades [22], as has bacterial sialidase [23]. The copper-containing galactose oxidase [24] and the bacterial methylamine dehydrogenase [25] which contain TTQ (tryptophan tryptophylquinone) instead of PQQ, both have seven blades. Proteins with eight blades include methanol dehydrogenases from both *M. extorquens* [8,12,26] and *Methylophilus* species [15,27], and nitrite reductase (V Fülöp, personal communication).

The 32  $\beta$ -strands that make up the superbarrel structure in MDH are labelled according to the 'W' motif in which they occur (1–8) and the position they take within the motif (strands A–D), strand A being closest to the pseudo eight-fold axis, with strand D on the surface of the subunit (Fig. 1). Using this nomenclature, the sequence of strands in the structure is the same as in the amino acid sequence (this is also seen in other superbarrel structures), with the sole exception of the final strand of the eighth motif (D8) which is derived from the N terminus, not the C terminus. This places sequences close to the C and N termini in strands C8 and D8 respectively, where they participate in the formation of a number of antiparallel  $\beta$ -type hydrogen bonds. A similar

pattern is seen in this region with neuraminidases and galactose oxidase, but not with methylamine dehydrogenase or nitrite reductase.

The conventional description of a superbarrel as being composed of four-stranded up-and-down  $\beta$ -sheet 'W' motifs needs some qualification when applied to the motifs in MDH. The major deviation from the ideal is in strand A which, while running more or less antiparallel to strand B, makes only three  $\beta$ -type hydrogen-bond interactions with it, all of which are close to the A–B strand turn (Fig. 3). Over most of its path, strand A is too far from strand B, and its peptide planes are in the wrong orientation for hydrogen-bond interactions with it. No other specific interactions seem to replace the missing A–B bonds, and it seems more likely that the conformations of the A strands are controlled by the close packing of side-chains around and across the pseudo eight-fold symmetry axis to fill the space in the very centre of the molecule. Near the centre of the  $\alpha$ -subunit, all eight strands come close together, and since five of these eight strands at the point of contact are glycines, close-packing is facilitated. The remaining B, C and D strands in each motif form a regular twisted  $\beta$ -sheet across sequences

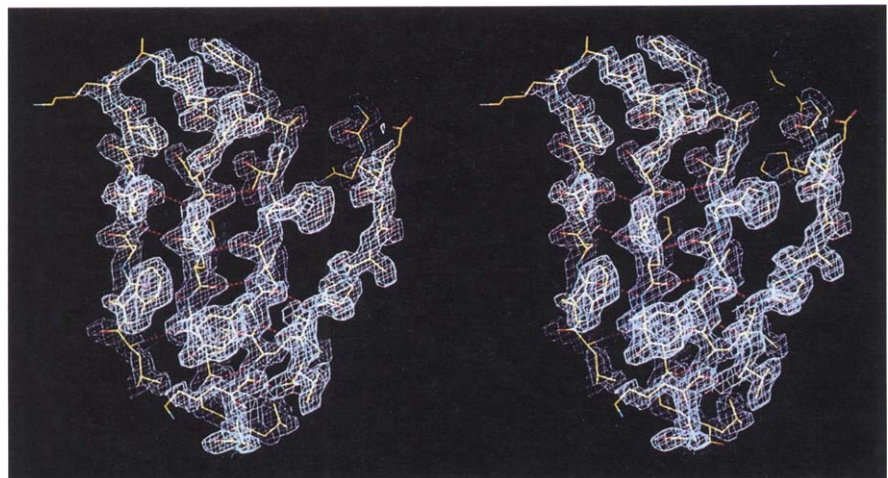


**Fig. 3.** A stereo drawing of the electron density associated with a typical 'W' motif of MDH.  $\beta$ -type hydrogen bonds within the unit are shown in broken red lines. The characteristic deviation of the A strand (right) from the regular  $\beta$ -sheet structure of strands B, C and D can be clearly seen. Fig. 1 shows the position of the 'W' motifs in the  $\alpha$ -subunit; the D strands are on the surface and the A strands nearer the centre.

eight to nine residues in length. In all motifs, the A–B and C–D corners are short and economical, but the B–C corners are more variable in length, forming extensions containing 24–30 residues in the cases of motifs 4, 6 and 8.

The  $\alpha$ -chain contains a total of three *cis* peptide bonds, stabilized by a ring of proline side chains (residues 72, 264 and 387). Pro72 is located in a very tight corner between the  $\beta$ -strands B1 and C1, Pro264 is in a longer loop between  $\beta$ -strands B4 and C4, while Pro387 is next to Cys386, which forms a normal intra-chain disulphide bridge with Cys415. A fourth unusual peptide bond is the non-planar *trans* peptide bond between adjacent cysteines in the active site (see below).

#### The tryptophan docking motif in the $\alpha$ -subunit

A novel type of interaction occurs in the  $\alpha$ -subunit through a consensus sequence of 11 residues, as shown in Fig. 4, in the C–D region of all W motifs except number 8. This gives rise to a common structure that can functionally be described as a tryptophan docking motif (Fig. 5). The two key components of this interaction are, firstly the peptide between residue 6 and the invariant glycine at position 7, which in any motif (Wn) is arranged parallel to, and in contact with, the indole ring of the tryptophan at position 11 in the previous motif (Wn–1), and secondly the main-chain carbonyl of residue 4 which makes a hydrogen bond with the indole NH group of this same tryptophan. These two peptides are held in position by hydrogen bonds involving the semi-invariant side chains at position 3 (Asp or Asn), position 6 (Thr) and position 8 (Asp/Glu). A further interaction involves the packing of the semi-invariant alanine at position 1 against the other side of the tryptophan at position 11 in its own motif (Wn). These interactions are illustrated in Figs 4 and 5, but exceptions to them

occur in motifs W1 and W7. In W1 the glycine at position 7 is replaced in the stacking interaction by proline at position 6; in W7 residue 1 (Ala498) does not form the expected interaction with Trp508.

The tryptophan docking motif recognizes the major characteristics of the tryptophan residue: its planar conjugated ring, and its ability to act as a hydrogen-bond donor through its ring NH group. It is interesting to note that the two exceptions to tryptophan in position 11 (Ser347 and Phe292) can only be involved in one of these two types of interaction, either stacking interactions or hydrogen bonds. Ser347 in W5 only makes a hydrogen bond with the peptide carbonyl of residue 4 in motif W6. In the other exception, Phe292 in W4 makes only stacking interactions, with the usual glycine peptide bond of W5 on one side, and a second glycine peptide bond in position 1 of W4.

Motif W8 is exceptional in having no consensus sequence (except for Trp44), and no C–D 'corner' because it comprises separate strands from the N-terminal and the C-terminal regions (Fig. 1). In this case there is an alternative docking motif involving only the D8 strand, which has no glycine to interact with the tryptophan in the previous motif. In its place there is a hydrophobic interaction between Trp508 and the side chain of Leu40. The carbonyl of this leucine (at position 7) also replaces the usual carbonyl at position 4 when forming a hydrogen bond with the tryptophan indole NH group.

Plotting the positions of the tryptophan docking motifs on the  $\alpha$ -chain shows that they make a planar, stabilizing girdle of interactions around the periphery of the  $\alpha$ -subunit (Fig. 6) in which the glycine peptide at one end of a reference motif interacts with the tryptophan in the previous

Position	1	2	3	4	5	-	6	7	8	9	10	11
<b>W1</b>	<b>Ala 77</b>	Leu	<b>Gly</b>	Leu	Asp	Asp	Pro	<b>Gly</b>	Thr	Ile	Leu	<b>Trp 88</b>
<b>W2</b>	<b>Ala 135</b>	Leu	<b>Asn</b>	Ala	Glu	-	<b>Thr</b>	<b>Gly</b>	<b>Glu</b>	Thr	Val	<b>Trp 145</b>
<b>W3</b>	<b>Ala 186</b>	Tyr	<b>Asp</b>	Val	Lys	-	<b>Thr</b>	<b>Gly</b>	<b>Glu</b>	Gln	Val	<b>Trp 196</b>
<b>W4</b>	Gly 282	Arg	<b>Asp</b>	Ala	Asp	-	<b>Thr</b>	<b>Gly</b>	<b>Glu</b>	Ala	Lys	<b>Phe 292</b>
<b>W5</b>	Thr 337	Leu	<b>Asp</b>	Arg	Thr	-	Asp	<b>Gly</b>	Ala	Glu	Val	<b>Ser 347</b>
<b>W6</b>	<b>Ala 457</b>	Tyr	<b>Asn</b>	Ala	Ile	-	<b>Thr</b>	<b>Gly</b>	<b>Asp</b>	Tyr	Lys	<b>Trp 467</b>
<b>W7</b>	<b>Ala 498</b>	Arg	<b>Asp</b>	Ser	Asp	-	<b>Thr</b>	<b>Gly</b>	<b>Asp</b>	Leu	Leu	<b>Trp 508</b>
<b>W8</b>	Val 577	Phe	Ser	Leu	Asp 581	-	Gln 39	Leu	Arg	Pro	Ala	<b>Trp 44</b>
<b>MDH Consensus</b>	<b>Ala</b>	X	<b>Asp/Asn</b>	X	X	-	<b>Thr</b>	<b>Gly</b>	<b>Asp/Glu</b>	X	X	<b>Trp</b>
<b>GDH/ADH Consensus</b>	<b>Ala</b>	X	<b>Asp/Asn</b>	X	X	-	<b>Thr</b>	<b>Gly</b>	<b>Lys</b>	X	X	<b>Trp</b>

**Fig. 4.** The consensus sequences in the tryptophan docking motif. The consensus sequence occurs at the C–D corners at the end of the C strands and the beginning of the D strands of each W motif; there are no loops between these strands. Positions 1–3 of the motif are at the end of the C strands and positions 6–11 or 7–11 are at the beginning of the D strands. The C–D corners are best characterized as four-residue ( $\beta$ ) turns or five-residue turns (comprising residues 3–6 or 3–7 respectively). Consensus sequences are also included for the quinohaemoprotein alcohol dehydrogenase (ADH) and glucose dehydrogenase (GDH), which is a membrane quinoprotein [47]. The Trp/Gly interaction in this motif in MDH was first mentioned by F Scott Mathews (in the 3rd Symposium on PQQ and Quinoproteins in Capri, 1994). The residues in bold show invariant or semi-invariant residues between motifs.

motif, and the tryptophan at the other end of the reference motif interacts with the glycine peptide of the succeeding motif (Fig. 5). The interactions around motifs W7 and W8 are augmented by further interactions at the  $\alpha$ - $\alpha$  interface. The presence of the 11-residue consensus sequence can most readily be explained if these motifs were derived by divergent evolution from an ancestral W motif containing such a sequence in its C-D corner. This observation contributes further data for the discussion of the evolution of superbarrel proteins [28]. We have not observed a similar tryptophan docking motif in the superbarrel proteins galactose oxidase and methyl-amine dehydrogenase. By contrast, the PQQ-containing dehydrogenases for glucose (GDH) and alcohol (ADH) show the greatest similarity to MDH in the sequences which form W motifs. In particular, they have a tryptophan docking motif at the C-D corners that is almost identical to that of MDH (Fig. 5) except that GDH and ADH contain lysine instead of asparagine or glutamate (Fig. 4). This is further evidence that these PQQ-containing quinoproteins have essentially similar overall structures to MDH.

#### Structure of the $\beta$ -subunit

The three-dimensional form of the 74 residue  $\beta$ -chain of MDH (Figs. 1 and 2) is most unusual in that it contains only local folds that form a very extended structure containing no hydrophobic core. The N-terminal 30

residues, which include one intra-chain disulphide bridge (Cys6-Cys12) and a proline-rich segment (residues 14-20), folded into a series of open turns. The 54 residues at the C-terminal end, which are rich in charged amino acids, are mostly located in a single straight  $\alpha$ -helix of 30 residues in seven turns, followed by a C-terminal segment folded back on the helix (Fig. 1). Overall, the  $\beta$ -chain forms a planar 'J'-shaped unit, with the long  $\alpha$ -helix as its stem, which hooks over the globular  $\alpha$ -subunit. The  $\beta$ -chain cannot be separated from the  $\alpha$ -chain without denaturation, but it seems probable that the three-dimensional structure of the  $\beta$ -chain is determined, to a considerable extent, by its interaction with the  $\alpha$ -chain. The  $\beta$ -chain does not participate in the active site of MDH, and in the absence of evidence of any other functional role, it is possible that the three-dimensional structure acts to stabilize the folded form of the large  $\alpha$ -chain. However, the lack of evidence for  $\beta$ -subunits in other PQQ-containing quinoproteins, perhaps indicates a more specific (unknown) role for this unusual subunit.

#### Subunit interactions

The  $\alpha$ -subunits contact one another in the region containing the D-strands of the seventh and eighth 'W' motifs. These D-strands do not, however, form anti-parallel hydrogen-bond interactions with their symmetry

**Fig. 5.** A stereo drawing of the structural motif between the strands C and D of a typical W unit which contains the 11-residue consensus sequence described in Fig. 4. The docking of this motif with the tryptophan (residue 88) at position 11 at the previous W unit can be seen in the extreme left. The equivalent tryptophan (residue 145) in the reference motif, which interacts with the succeeding W, is at the extreme right.

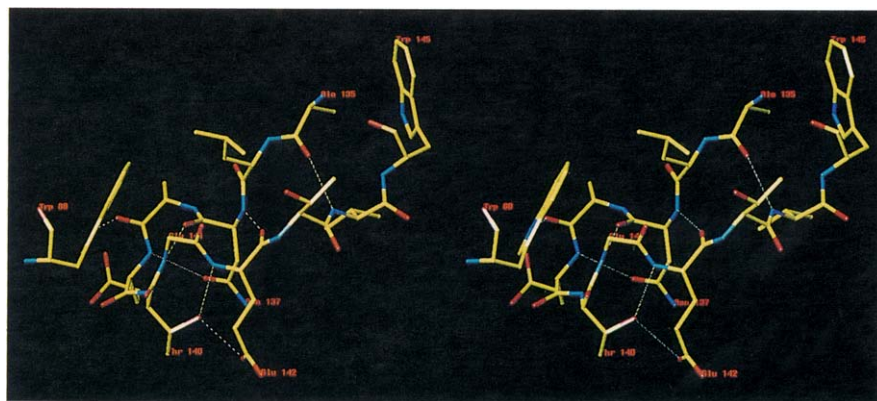
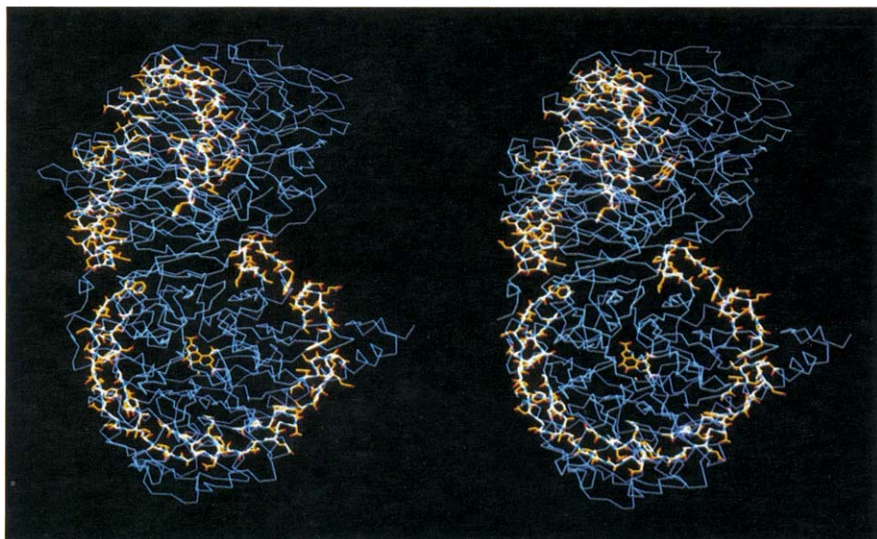


**Fig. 6.** A stereo drawing of the MDH tetramer showing the girdle of tryptophan docking motifs around each  $\alpha$ -subunit. The molecular two-fold axis is inclined at about 45° to demonstrate the circular, planar nature of the girdle.



equivalents, as observed with the nitrite reductase dimer (V Fülöp, personal communication). Instead, the  $\alpha$ -chains interact over a large planar interface containing many hydrophobic and hydrophilic side-chain interactions. These interactions are augmented by the 10 residues C-terminal to the  $\alpha$ -chains which form an extension that associates with the symmetry-related subunit, again through hydrophobic and hydrophilic interactions. The J-shaped  $\beta$ -chain runs across the surface of the much larger  $\alpha$ -subunit and makes contact along its entire length. The  $\beta$ -chain is neither buried in the surface of the  $\alpha$ -chain (Figs 1 and 2) nor associated so as to extend any of the  $\alpha$ -chain structures. Although some hydrophobic interactions occur between the  $\alpha$ - and  $\beta$ -subunits, ion-pair interactions seem to predominate, an observation that may be related to the fact that 39% of the  $\beta$ -chain residues are charged. The  $\beta$ -chain makes contact with the edges of the W1–W4 motifs of the  $\alpha$ -chain with ion-pair interactions involving Glu148, Glu193, Arg197, Lys236, Glu267 and Glu301 of the  $\alpha$ -chain, and Lys16, Glu48, Arg50, Arg54 and Lys59 of the  $\beta$ -chain.

#### The active site

The active site of MDH is located in an internal chamber entirely within each  $\alpha$ -subunit. It is located approximately on the pseudo eight-fold symmetry axis, at the end of the superbarrel structure which contains the loops between the B and C strands of motifs W6 and W8. These fold over the end of the superbarrel to enclose the active-site chamber (Fig. 1). Surface-accessible residues in these folds form a funnel-shaped depression in the surface of the  $\alpha$ -subunit. A remarkable feature of the 'funnel' is that its residues are almost exclusively hydrophobic (surface residues in bold type):

100-**AVACCDL**;420-**PFMLP**;430-**FFV**;  
540-**WPGVGLVFDLADPTAGL**

At the base of the funnel is the narrow entrance to the active-site chamber in which are located the non-covalently bound PQQ prosthetic group, a bound  $\text{Ca}^{2+}$ , the Cys103–Cys104 disulphide bridge and a potential base Asp303, in addition to a number of bound water molecules. There is no indication from structural studies of any obvious involvement of the  $\beta$ -chain, or the symmetry-related  $\alpha\beta$ -unit in the active site. However, we know little of the structural requirements of electron transfer to

cytochrome  $c_L$ , except that ionic interactions between lysyl residues on the  $\alpha$ -chain and carboxylates on the cytochrome  $c_L$  are involved in the 'docking' process [29].

#### The novel disulphide ring structure

Methanol dehydrogenase is the first active enzyme whose X-ray structure indicates formation of a disulphide bridge between two adjacent cysteine residues, a structure requiring considerable distortion for its formation. Both *cis*- and non-planar configurations of the linking peptide have been proposed from energy considerations [13,14]. Although only the *cis*-peptide distortion has been observed in the X-ray structure of Cys–Cys dipeptides in which the disulphide link is present [30,31], it is possible that the *trans* isomer might have been present but lost in the crystallization process. Furthermore, an NMR study of a heptapeptide containing adjacent cysteines showed that up to 30% of the sample contained a *trans* peptide bond [32]. The electron density around Cys103 and Cys104 in MDH from *M. extorquens* in a multiple isomorphous replacement (MIR) map at 3 Å resolution [12] was satisfactorily fitted by the structure of cyclo-L-cysteine [31], which has a planar *cis*-peptide link. However, the greater resolution of the present fully refined electron-density map at 1.94 Å, in which the electron density around the bridge has been generated from structure factors that exclude the atoms of residues 103 and 104, shows clearly that the linking peptide has a *trans* configuration, and that the distortion is in fact taken up in a non-planar configuration of this peptide (Fig. 7).

Because the Cys103–Cys104 disulphide bridge has a non-standard structure, we made a best fit of the atoms to the electron density. The two sulphur atoms were resolved from one another at high electron-density values. These and the other atoms of the eight-membered ring were fitted using the program 'O' [33] (Fig. 7). It can be seen that the electron density indicates a non-planar configuration for the linking peptide group. The non-planarity was taken up entirely in the model at the carbonyl carbon, as suggested by the electron density. The fit shown in Fig. 7 has an  $\omega$  of 145°, giving a distortion from planarity of 35°. None of the bond lengths and other bond angles in the novel eight-membered disulphide ring could be distinguished from their standard values in the observed electron density. Thus, on the basis of the current 1.94 Å electron-density map, the

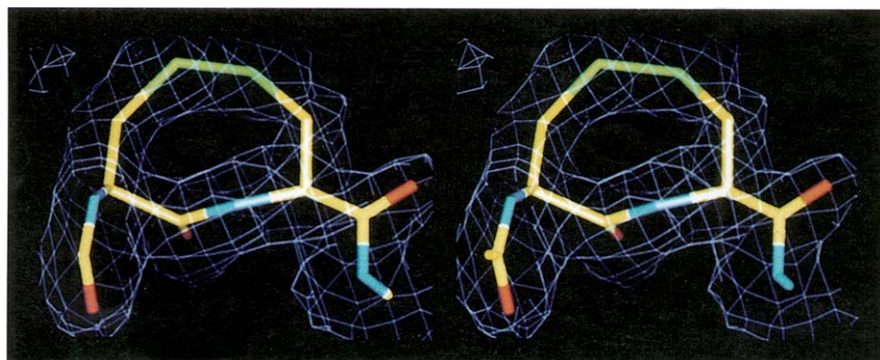


**Fig. 7.** A stereo drawing of the electron density around the Cys103–Cys104 disulphide bridge and the interpretation of the feature with a non-planar linking peptide bond, giving a novel eight-membered ring structure.

only distortion observed in the disulphide ring is the deviation from planarity by 35° in the linking peptide bond. This demonstrates that the distortion in the polypeptide chain within the disulphide ring structure is of a different nature from that observed in the isolated model Cys–Cys dipeptides.

#### *The interactions of PQQ and Ca<sup>2+</sup> in the active site*

The interactions of the PQQ with MDH (see Figs 8 and 9) can be best described in terms of two non-polar interactions with either side of the PQQ ring system (the axial interactions), and a number of polar and ionic interactions with the substituent groups (carboxyl and quinones), of the PQQ prosthetic group (the equatorial interactions). The PQQ ring is sandwiched between the indole ring of Trp243, which is within 15° of coplanarity with the PQQ ring and in contact with it, and the two sulphur atoms of the disulphide bridge whose separation from the PQQ ring atoms of 3.75 Å also indicates an interaction. A considerable number of amino acid residues are involved in the equatorial interactions which involve the substituent groups of the PQQ ring system. These interactions are exclusively hydrogen bond and ion-pair interactions, involving residues mostly on the A strands of the W motifs. These include Glu55, Arg109, Thr159, Ser174, Thr 241, Arg331, Asn394 and Trp476 as shown in Fig. 8. Of particular interest are the interactions of the C4 and C5 oxygen atoms; the electron density-maps show that whereas the C5 oxygen is in the plane of the PQQ ring system, the C4 oxygen is out of the plane by about 40°, consistent with the semiquinone state of PQQ [9,11]. Both C4 and C5 oxygens are hydrogen bonded by the NH<sub>1</sub> and NH<sub>2</sub> atoms respectively of Arg331, and in addition the C4 oxygen makes a longer hydrogen-bond interaction with the amide NH<sub>2</sub> of Asn394 whose amide CO is hydrogen-bonded to its own main-chain NH group. The bonding of the C4 and C5 oxygen atoms is likely to be maintained in the fully oxidized quinone and fully reduced quinol forms of the prosthetic group. Arg331 also makes hydrogen bonds between its NH<sub>2</sub> and the carboxylate and main-chain carbonyl of Asp303. The two side chains lie side by side, permitting free access to the carboxyl group of Asp303, which is the most likely candidate for the base required by some catalytic mechanisms previously proposed for MDH [2,8].

**Fig. 9.** A stereo drawing of the active site of MDH centred on the likely substrate binding site. The PQQ, sandwiched between Trp243 and the novel ring structure formed by the Cys103–Cys104 disulphide bridge, can be seen at the top left. The Ca<sup>2+</sup> is shown as a yellow sphere ligated by the O5, N6 and O7 of PQQ, and the side chains of Glu177 and Asn261. We suggest that the proposed 'essential' base is Asp303 which is shown at centre right. This active-site region is similar to that seen in the lower resolution structure of MDH from *Methylophilus* W3A1 [27].

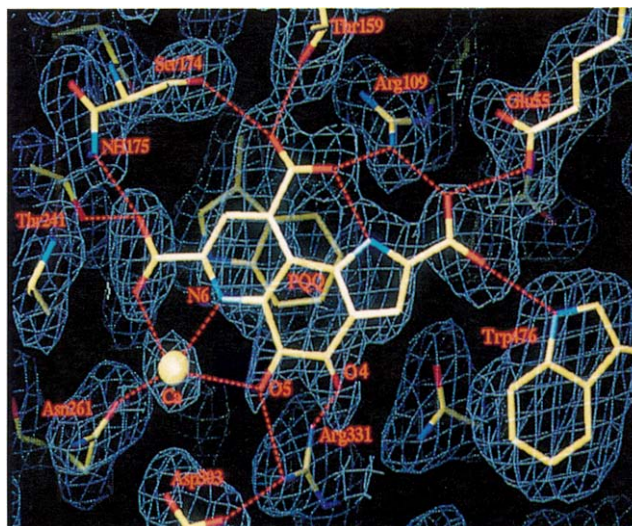
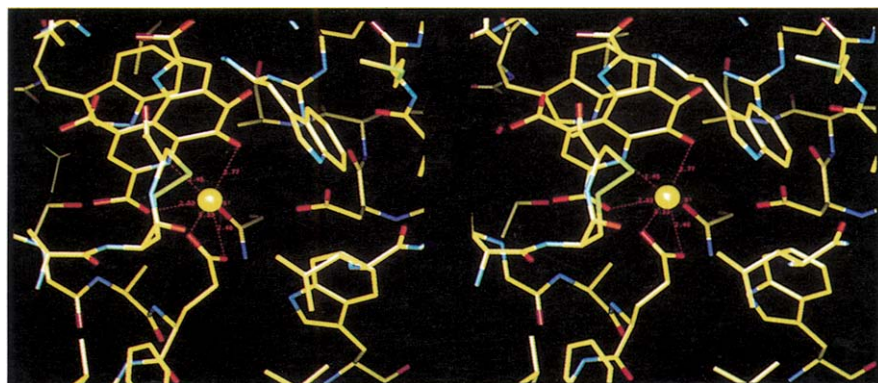


**Fig. 8.** A view of the electron density around the PQQ from an omit-map which excluded the prosthetic groups from the model. Carbon atoms are in yellow, oxygens in red and nitrogens in blue. The associated Ca<sup>2+</sup> is shown as a yellow ball. Protein residues that interact with the PQQ are labelled, and hydrogen bonds and calcium interactions are shown by dotted lines. The proposed catalytic base, Asp303, is also shown.

The coordination sphere of the calcium ion in the active site contains both protein and PQQ atoms (Fig. 9). The protein atoms include both oxygens from the carboxylate of Glu177 and the amide oxygen of Asn261. The PQQ atoms include the C5 quinone oxygen, one oxygen of the C7 carboxylate and, surprisingly, the N6 ring atom which is only 2.45 Å from the metal ion. The five oxygen ligands have distances from the metal of 2.4–2.8 Å. There are two water molecules near the Ca<sup>2+</sup> in the active site; one is bound by six hydrogen bonds to protein groups and is 3.76 Å from the calcium, while the other water is bound to the carboxylate group of Asp303 and is 3.3 Å from the calcium. Neither of these waters is a primary calcium ligand.

#### *The mechanism of MDH*

The interaction between the Ca<sup>2+</sup> and the C5 quinone group is of particular interest, because the C5 oxygen has been demonstrated to be very reactive towards nucleophiles, a property that may suggest C5 to be the site of a covalent PQQ–substrate complex [1,3,34,35] (for



reviews see [2,8]). Asp303 is very close to the C5, where it could act as a base, initiating the reaction by abstracting a proton from the alcohol substrate. In this mechanism, the  $\text{Ca}^{2+}$  ion could act as a Lewis acid providing the electrophilic C5 for attack by an oxyanion or hydride through its coordination with the C5 carboxyl oxygen. In this way, the calcium could play a dual role in structure and catalysis, as suggested for example, in phospholipase A2 [36]. The mediation of the disulphide bridge in the transfer of electrons from the reduced form of PQQ to cytochrome  $c_L$  has been suggested earlier [12,26], but an alternative or additional role of the disulphide ring might be the protection or stabilization of the free-radical semiquinone form of the prosthetic group demonstrated here. Further work on substrate interactions and reduced and oxidized forms of MDH is required, but the active-site features described here are satisfyingly close to those expected from mechanistic proposals for quinoprotein dehydrogenation and electron transfer.

### Biological implications

**By analogy with flavins and flavoproteins, the term quinoprotein was first coined in ~1980 to include proteins containing pyrroloquinoline quinone (PQQ). Quinoprotein dehydrogenases share with flavoproteins the fascinating problem of transferring electrons through, and between, proteins. Methanol dehydrogenase (MDH) was the first PQQ-containing dehydrogenase to have its structure determined, the high-resolution structure presented here being an essential step in understanding both the electron transfer process and the basic mechanism of action of quinoprotein dehydrogenases. Understanding will, however, be complicated by the fact that the electron acceptor for MDH is cytochrome  $c_L$ , whereas the electron acceptor for the alcohol dehydrogenase of acetic acid bacteria which is haem C, present on a separate domain of its heavy chain, and the electron acceptor for the membrane glucose dehydrogenase is ubiquinone.**

**A number of features seen in our high-resolution structure are of general interest in the study of the quinoprotein dehydrogenases. The novel tryptophan docking site that stabilizes the eight-fold symmetry of the 'propeller fold' in the  $\alpha$ -subunit is also likely to be a feature of the dehydrogenases for alcohol and glucose, as indicated by the extent of sequence similarity in these regions. These proteins are all  $\text{Ca}^{2+}$ -dependent and the conservation of amino acids to which  $\text{Ca}^{2+}$  is coordinated in MDH indicates similar active sites. The adjacent cysteines of the novel disulphide ring are also present in alcohol dehydrogenase, but not in glucose dehydrogenase suggesting that this structure does not have a role in electron transfer from the reduced quinol form of the prosthetic group to the membrane ubiquinone. That**

**reaction is a two-electron transfer and so an alternative role of the disulphide ring might be to stabilize the non-planar semiquinone form of the PQQ seen in MDH but which is not necessary in glucose dehydrogenase.**

### Materials and methods

#### Crystallization

MDH from *M. extorquens* was purified and crystallized as described previously [18]. The enzyme crystallized predominantly in an orthorhombic form. These crystals diffracted very well, beyond 1.9 Å in synchrotron radiation and to 2.5 Å in the in-house Rigaku RU200 generator. They were readily grown but suffered severely from twinning; single crystals of suitable size rarely grew. Under very similar crystallization conditions, sometimes in the same drop, another type of crystal could be grown; these belonged to the triclinic class and diffracted beyond 2 Å in the in-house X-ray generator.

#### Orthorhombic crystals

*Data collection and structure determination:* The structure was solved by the MIR method using orthorhombic crystals. These belonged to the space group  $P2_12_1$  and the unit cell parameters were  $a=66.8$  Å,  $b=108.9$  Å,  $c=189.2$  Å, with one  $\alpha_2\beta_2$  tetramer in the asymmetric unit. Collection of native data (2.5 Å) and the initial screening for suitable heavy-atom derivatives were done in the in-house Siemens/Xentronics multiwire area detector [37,38]. The derivative data sets (5.5 Å) produced interpretable Patterson maps and the main binding sites of the heavy-atoms were easily identified, and heavy-atom difference Fourier maps showed the rest of the heavy-atom binding sites. However, the phasing power of the individual derivatives was small (Table 1). The low resolution map showed that the molecule was composed of two compact units related by a two-fold crystallographic symmetry axis which was determined from the heavy-atom binding sites which occurred in pairs [18].

In the next stage, native and derivative data were collected using the in-house MAR-research imaging plate detector mounted on a Rigaku RU200 generator. The crystals diffracted well beyond 2.5 Å but the data were limited to 3.0 Å by the lack of resolution of spots along the long  $c$ -axis. The oscillation range of one image was typically 0.75° and data were collected for >90° while the crystals were rotated approximately about the shortest  $a$ -axis, the needle axis of the crystals. The data were autoindexed [39] using programs IMSTILLS and REFIX from the CCP4 program package [SERC (UK) Collaborative Computing Project no. 4, Daresbury Laboratory, UK, 1979] and then processed by DENZO and SCALEPACK [40]. Refinement of heavy-atom positions and phasing were done by MLPHARE [41] from the 12 heavy-atom binding sites and using all the data between 20–3 Å. The average figure of merit considering all reflections was 0.47. Phases were improved by solvent flattening [42] and symmetry-averaging by using GAP (J Grimes and DI Stuart, unpublished program) and O [33] in combination with CCP4 programs of Fourier calculation and phase combination. Maps were calculated at 3.0 Å resolution using these improved phases and were used to build the model of the molecule. This was done initially by putting markers along the continuous trace of density on a stack map on transparencies and then using these markers to build the backbone of the molecule on an Evans and Sutherland ESV workstation using the interactive graphics program FRODO

**Table 1.** Data collection and refinement statistics.

Dataset	Concentration	Maximum resolution (Å)	Unique reflections (% complete)	R <sub>merge</sub> (%)	MFID (%)	Number of sites	Phasing statistics  F <sub>H</sub>   E (all data)	R <sub>c</sub> (%)
Native <sup>a</sup>		2.75	31 542 (87%)	7.9				
EMP <sup>a</sup>	23 mM	5.0	5131 (82%)	5.4	12.1	4	1.57	43
K <sub>2</sub> PtCl <sub>6</sub> <sup>a</sup>	24 mM	5.0	3820 (61%)	6.3	17.5	4	1.51	50
K <sub>2</sub> PtCl <sub>5</sub> <sup>a</sup>	20 mM	5.4	3901 (79%)	6.3	10.6	5	1.54	45
PCMBS <sup>a</sup>	Saturated	5.4	3118 (65%)	6.6	9.4	4	1.46	58
Native <sup>b</sup>		3.0	27 298 (96%)	6.2				
K <sub>2</sub> PtCl <sub>6</sub> <sup>b</sup>		3.0	26 854 (95%)	9.3	13.9	4	1.58	52
EMP <sup>b</sup>		3.0	26 500 (94%)	6.6	10.9	4	1.50	53
Native <sup>c</sup>		1.94	91 350 (86%)	5.4				

Abbreviations: EMP, ethylmercuric phosphate; PCMBS, *p*-chloromercuric benzene sulphonic acid. <sup>a</sup>Orthorhombic crystals, Siemens/Xentronics; <sup>b</sup>orthorhombic crystals, image plate; <sup>c</sup>triclinic crystals, image plate.  $R_{\text{merge}} = \frac{\sum (|I_j - \langle I_j \rangle|)}{\sum \langle I_j \rangle}$ , where  $I_j$  is the intensity of an observation of reflection  $j$  and  $\langle I_j \rangle$  is the average intensity for reflection  $j$ . MFID = mean fractional isomorphous difference,  $\frac{\sum ||F_{\text{PH}}| - |F_{\text{P}}||}{\sum |F_{\text{P}}|}$  where  $|F_{\text{P}}|$  and  $|F_{\text{PH}}|$  are the structure amplitudes of the native and the derivative respectively.  $R_c = \frac{\sum |F_{\text{H}(\text{o})}| - \sum |F_{\text{H}}|}{\sum |F_{\text{H}(\text{o})}|}$ , where  $|F_{\text{H}(\text{o})}|$  and  $|F_{\text{H}}|$  are observed and calculated heavy-atom structure-factor amplitudes.  $|F_{\text{H}}|/E$  = phasing power,  $E$  is the residual lack of closure error.

[43] and O [33]. About 75% of the residues on the  $\alpha$ -chain could then be identified and fitted at this stage using the sequences of the  $\alpha$ - and  $\beta$ -subunits [19,20]. The prosthetic group was located at the centre of the  $\alpha$ -subunit in the flat area of density not connected to the protein chain and just large enough to accommodate PQQ. Close to this, the Ca<sup>2+</sup> was identified in another isolated piece of density in an appropriate environment. The unusual disulphide bridge between residues Cys103–Cys104 was also seen in this same region close to the prosthetic group. The density was poor in certain regions of the map, such as the regions, near the termini, and in one of the extended long loops, which was therefore built as a polyaniline chain. The residues at the termini were not included in the first stage of refinement. For the  $\beta$ -chain, the long helix at the C terminus and part of the N terminus were built but there was no density connecting the two ends.

**Refinement:** This initial model was refined using X-PLOR [44] which consisted of positional refinement followed by simulated annealing, where the temperature of the system was increased to 4000 K, then allowed to cool down to 300 K in 50 K decrements using time steps of 0.5 fsec at each temperature. All 27 983 reflections in the resolution range 8–3 Å were included. Non-crystallographic symmetry restraint was maintained throughout the refinement. The process of refinement was monitored by calculating  $R_{\text{free}}$  [45] for a subset of 5% of the data. This model was then manually rebuilt, about 94% of the residues then being included. This was subject to another round of positional refinement and simulated annealing, followed by B-factor refinement. The R-factor at this stage was 32.4% (26 571 reflections) while  $R_{\text{free}}$  was 40.8% (1412 reflections). The model could not be improved any further on the basis of this 3 Å map. It was used as a search model to solve the structure in the triclinic cell by molecular replacement.

#### Triclinic crystals

**Data collection and structure determination:** The triclinic crystals have the unit cell parameters  $a=61.16$  Å,  $b=72.19$  Å,  $c=86.17$  Å,  $\alpha=86.21^\circ$ ,  $\beta=76.09^\circ$ ,  $\gamma=70.44^\circ$  and the unit cell contained one  $\alpha_2\beta_2$  tetrameric molecule. Native X-ray data of the triclinic crystals were collected using the in-house MAR-research

imaging plate. The triclinic crystals, like the orthorhombic ones, diffracted very well, and the smaller cell dimension allowed the data to be collected up to 1.94 Å. A cross-rotation function was calculated by the real-space Patterson search method as employed in X-PLOR. Reflections between 15–4 Å were used and the search model was placed in an orthogonal cell of triclinic symmetry of dimensions  $a=b=c=220$  Å. All Patterson vectors of length 10–60 Å were examined. The solution was unambiguous and appeared as the highest peak over a wide range of search. A translation was not necessary as the space group symmetry of the structure solved was P1.

**Refinement:** This model was subjected to rigid-body refinement including all 90 046 reflections in the resolution range 8 Å–1.94 Å. The initial R-value was 46.1%. The model was fitted in the electron-density map using the program O. The map was of excellent quality. It was possible to build the missing regions which were either left out, or included as polyanilines, in the previous models by correctly identifying the residues. Repeated cycles of refinement followed by manual fitting of the model into the electron density maps were carried out. Throughout the refinement a restraint on non-crystallographic symmetry was maintained between the two  $\alpha\beta$  units and the free R-factor was calculated with 5% (4502 reflections) of the data. After the R-value dropped below 25%, water molecules were placed in the  $F_o - F_c$  peaks above  $3\sigma$  and at chemically acceptable sites using WATERADD (S Knight, unpublished program) and after visual verification on the  $F_o - F_c$  map. These water molecules were added in successive steps and were included in the subsequent refinement cycles. The final model consists of 595 residues of the  $\alpha$ -chain and 73 of the  $\beta$ -chain; the extreme ends (C termini) of neither chain could be placed (10 out of a total of 1336 residues in the  $\alpha_2\beta_2$  tetramer). Bulk solvent correction was applied so that the low resolution (20–8 Å) data could be incorporated in the refinement. The R-factor of 19.85% was attained for 10 412 protein atoms and 638 water molecules considering all reflections in the range 10–1.94 Å (Table 2). The stereochemistry of the model was good, the rms deviation from identity being 0.008 Å for bond distances and  $1.596^\circ$  for bond angles, considering all the 91 359 reflections in the range 10–1.94 Å. A Ramachandran analysis of the

**Table 2.** Model refinement statistics.

No. of non-hydrogen protein atoms	10 412
No. of solvent sites	638
Missing residues	10
Average B-value <sup>a</sup>	16.0 Å <sup>2</sup> and 16.4 Å <sup>2</sup>
Resolution limits	20–1.94 Å
R-factor	19.85
No. of reflections	86 729
Free R-factor	22.93
No. of reflections	4621
Rms deviation in bond lengths	0.008 Å
Rms deviation in bond angles	1.596°

<sup>a</sup>Average B-value for two  $\alpha\beta$  units.

main-chain conformation shows that 88% of the residues are in the most favoured region, while six non-glycine residues in the whole  $\alpha_2\beta_2$  tetramer are in the disallowed region as defined in PROCHECK [46]. The residues in the disallowed zone were all found to be in very good density.

Atomic coordinates are being deposited with the Brookhaven Protein Data Bank.

**Acknowledgements:** We wish to thank Mr G Cozier (Biochemistry Department, Southampton) and Dr M Noble, Dr S Gover, Dr M Sunde, Mr P Rowland (Laboratory of Molecular Biophysics) for helpful discussions at various stages of the work and Mr S Lee and Mr A May for assistance with the figures. We acknowledge financial support from the SERC, The Wellcome Trust and the Oxford Centre for Molecular Sciences, University of Oxford (KH).

## References

- Anthony, C. (1986). The bacterial oxidation of methane and methanol. *Adv. Microb. Physiol.* **27**, 113–210.
- Anthony, C. (1993). Methanol dehydrogenase in Gram-negative bacteria. In *Principles and Applications of Quinoproteins*. (Davidson, V.L., ed), pp. 17–45, Marcel Dekker, New York.
- Duine, J.A., Frank, J. & Jongejan, J.A. (1987). Enzymology of quinoproteins. In *Advances in Enzymology*. pp. 169–212, John Wiley & Sons, New York.
- Duine, J.A., Frank, J. & de Beer, R. (1984). An electron-nuclear double-resonance study of methanol dehydrogenase and its coenzyme radical. *Arch. Biochem. Biophys.* **233**, 708–711.
- Anthony, C. (1992). The c-type cytochromes of methylotrophic bacteria. *Biochim. Biophys. Acta* **1099**, 1–15.
- Frank, J., van Krimpen, S.H., Verwiël, P.E.J., Jongejan, J.A., Mulder, A.C. & Duine, J.A. (1989). On the mechanism of inhibition of methanol dehydrogenase by cyclopropane-derived inhibitors. *Eur. J. Biochem.* **184**, 187–195.
- Frank, J., Dijkstra, M., Balny, C., Verwiël, P.E.J. & Duine, J.A. Methanol dehydrogenase: mechanism of action. In *PQQ and Quinoproteins*. (Jongejan, J.A. and Duine, J.A., eds.), pp. 13–22, Kluwer Academic Publishers, Dordrecht, The Netherlands.
- Anthony, C., Ghosh, M. & Blake, C.C.F. (1994). The structure and function of methanol dehydrogenase and related PQQ-containing quinoproteins. *Biochem. J.* **304**, 665–674.
- Frank, J., Dijkstra, M., Duine, A.J. & Balny, C. (1988). Kinetic and spectral studies on the redox forms of methanol dehydrogenase from *Hyphomicrobium X*. *Eur. J. Biochem.* **174**, 331–338.
- Dijkstra, M., Frank, J. & Duine, J.A. (1989). Studies on electron transfer from methanol dehydrogenase to cytochrome  $c_1$ , both purified from *Hyphomicrobium X*. *Biochem. J.* **257**, 87–94.
- Richardson, I.W. & Anthony, C. (1992). Characterization of mutant forms of the quinoprotein methanol dehydrogenase lacking an essential calcium ion. *Biochem. J.* **287**, 709–715.
- Blake, C.C.F., Ghosh, M., Harlos, K., Avezoux, A. & Anthony, C. (1994). The active site of methanol dehydrogenase contains a disulphide bridge between adjacent cysteine residues. *Nat. Struct. Biol.* **1**, 102–105.
- Ramachandran, G.N. & Sasisekharan, V. (1968). Conformation of polypeptides and proteins. *Adv. Protein Chem.* **23**, 283–437.
- Chandrasekaran, R. & Balasubramanian, R. (1969). Stereochemical studies of cyclic peptides. VI. Energy calculations of the cyclic dipeptide cysteinyl-cysteine. *Biochim. Biophys. Acta* **188**, 1–9.
- Xia, Z.X., et al., & Mathews, F.S. (1992). The three-dimensional structures of methanol dehydrogenase from 2 methylotrophic bacteria at 2.6 Å resolution. *J. Biol. Chem.* **267**, 22289–22297.
- Chen, L.Y., Mathews, F.S., Davidson, V.L., Huizinga, E.G., Vellieux, F.M.D. & Hol, W.G.J. (1992). Three-dimensional structure of the quinoprotein methylamine dehydrogenase from *Paracoccus denitrificans* determined by molecular replacement at 2.8 Å resolution. *Proteins* **14**, 288–299.
- Murzin, A.G. (1992). Structural principles for the propeller assembly of  $\beta$ -sheets: the preference for seven-fold symmetry. *Proteins* **14**, 191–201.
- Ghosh, M., Harlos, K., Blake, C.C.F., Richardson, I. & Anthony, C. (1992). Crystallization and preliminary crystallographic investigation of methanol dehydrogenase from *Methylobacterium extorquens* AM1. *J. Mol. Biol.* **228**, 302–305.
- Anderson, D.J., Morris, C.J., Nunn, D.N., Anthony, C. & Lidstrom, M.E. (1990). Nucleotide sequence of the *Methylobacterium extorquens* AM1 *moxF* and *moxJ* genes involved in methanol oxidation. *Gene* **90**, 173–176.
- Nunn, D.N., Day, D.J. & Anthony, C. (1989). The second subunit of methanol dehydrogenase of *Methylobacterium extorquens* AM1. *Biochem. J.* **260**, 857–862.
- Branden, C. & Tooze, J. (1991). *Introduction to Protein Structure*, p. 64, Garland Publishing Co., New York.
- Varghese, J.N., Laver, W.G. & Colman, P.M. (1983). Structure of the influenza virus glycogen antigen neuraminidase at 2.9 Å resolution. *Nature* **303**, 35–40.
- Crennell, S.J., Garman, E.F., Laver, W.G., Vimr, E.R. & Taylor, G.L. (1993). Crystal structure of a bacterial sialidase (from *Salmonella typhimurium* LT2) shows the same fold as an influenza virus neuraminidase. *Proc. Natl. Acad. Sci. USA* **90**, 9852–9856.
- Ito, N., Phillips, S.E.V., Yadav, K.D.S. & Knowles, P.F. (1994). Crystal structure of a free radical enzyme, galactose oxidase. *J. Mol. Biol.* **238**, 794–814.
- Vellieux, F.M.D., et al., & Hol, W.G.J. (1989). Structure of quinoprotein methylamine dehydrogenase at 2.25 Å resolution. *EMBO. J.* **8**, 2171–2178.
- Ghosh, M., Avezoux, A., Anthony, C., Harlos, K., & Blake, C.C.F. (1994). X-ray structure of PQQ-dependent methanol dehydrogenase. In *Towards a Molecular Basis of Alcohol Use and Abuse*. (Jansson, B., Jornvall, H., Rydberg, U., Terenius, L., & Vallée, B.L., eds), pp. 251–260, Birkhäuser Verlag, Basel.
- White, S., et al., & Davidson, V.L. (1993). The active site structure of the calcium-containing quinoprotein methanol dehydrogenase. *Biochemistry* **32**, 12955–12958.
- Bork, P. & Doolittle, R.F. (1994). *Drosophila* kelch motif is derived from a common enzyme fold. *J. Mol. Biol.* **236**, 1277–1282.
- Cox, J.M., Day, D.J. & Anthony, C. (1992). The interaction of methanol dehydrogenase and its electron acceptor, cytochrome  $c_1$ , in the facultative methylotroph *Methylobacterium extorquens* AM1 and in the obligate methylotroph *Methylophilus methylotrophus*. *Biochim. Biophys. Acta* **1119**, 97–106.
- Capasso, S., Mattia, C. & Mazzarella, L. (1977). Structure of a cis-peptide unit: molecular conformation of the cyclic disulphide L-cysteinyl-L-cysteine. *Acta Crystallogr. B* **33**, 2080–2083.
- Mez, H.-C. (1974). Cyclo-L-cystine acetic acid. *Cryst. Struct. Commun.* **3**, 657–660.
- Sukumaran, D.K., Prorok, M. & Lawrence, D.S. (1991). A molecular constraint that generates a cis peptide bond. *J. Am. Chem. Soc.* **113**, 706–707.
- Jones, T.A., Zou, J.Y., Cowan, S.W. & Kjeldgaard, M. (1991). Improved methods for building protein models in electron density maps and the location of errors in these models. *Acta Crystallogr. A* **47**, 110–119.
- Dekker, R.H., Duine, J.A., Frank, J., Verwiël, P. & Westerling, J. (1982). Covalent addition of water, enzyme substrates and activators to pyrroloquinoline quinone, the coenzyme of quinoproteins. *Eur. J. Biochem.* **125**, 69–73.
- Itoh, S., et al., & Kasai, N. (1993). C-4 and C-5 adducts of cofactor PQQ (pyrroloquinoline quinone) — model studies directed toward the action of quinoprotein methanol dehydrogenase. *J. Am. Chem. Soc.* **115**, 9960–9967.
- Scott, D.L., White, S.P., Otwinowski, Z., Yuan, W., Gelb, M.H. & Sigler, P.B. (1990). Interfacial catalysis: the mechanism of phospholipase A2. *Science* **250**, 1541–1546.

37. Durbin, R.M., *et al.*, & Wiley, D.C. (1986). Protein, DNA and virus crystallography with a focussed imaging proportional counter. *Science* **232**, 1127–1132.
38. Blum, M., Metcalf, P., Harrison, S.C. & Wiley, D.C. (1987). A system for the collection and on-line integration of X-ray diffraction data from a multi-wire area detector. *J. Appl. Crystallogr.* **20**, 235–242.
39. Kabsch, W. (1988). Automatic indexing of rotation diffraction patterns. *J. Appl. Crystallogr.* **21**, 67–71.
40. Otwinowski, Z. (1993). DENZO: An Oscillation Data Processing Program for Macromolecular Crystallography, Yale University, New Haven, CT.
41. Otwinowski, Z. (1991). Maximum likelihood refinement of heavy atom parameters. In *Isomorphous Replacement and Anomalous Scattering*, pp. 80–86, Daresbury Laboratory, Warrington, UK.
42. Wang, B.C. (1985). Resolution of phase ambiguity in macromolecular crystallography. *Methods Enzymol.* **115**, 90–112.
43. Jones, T.A. (1985). Interactive computer graphics: FRODO. *Methods Enzymol.* **115**, 157–171.
44. Brünger, A.T. (1992). X-PLOR Manual version 3.3: A system for crystallography and NMR. Yale University, New Haven, CT.
45. Brünger, A.T. (1992). The free R-value: a novel statistical quantity for assessing the accuracy of crystal structures. *Nature* **355**, 472–474.
46. Laskowski, R.A., MacArthur, M.W., Moss, D.S. & Thornton, J.M. (1993). PROCHECK: a program to check the stereochemical quality of protein structures. *J. Appl. Crystallogr.* **26**, 283–291.
47. Anthony, C. (1992). The structure of bacterial quinoprotein dehydrogenases. *Int. J. Biochem.* **24**, 29–39.

Received: 1 Dec 1994; revisions requested: 19 Dec 1994;  
revisions received: 9 Jan 1995. Accepted: 12 Jan 1995.